Aftershocks in a frictional earthquake model

O. M. Braun

Institute of Physics, National Academy of Sciences of Ukraine, 46 Science Avenue, 03028 Kiev, Ukraine,
and International School for Advanced Studies (SISSA), Via Bonomea 265, 34136 Trieste, Italy

Erio Tosatti

International School for Advanced Studies (SISSA), Via Bonomea 265, 34136 Trieste, Italy;
CNR-IOM Democritos National Simulation Center, Via Bonomea 265, 34136 Trieste, Italy;
and International Centre for Theoretical Physics (ICTP), Strada Costiera 11, 34151 Trieste, Italy

Inspired by spring-block models, we elaborate a "minimal" physical model of earthquakes which reproduces two main empirical seismological laws, the Gutenberg-Richter law and the Omori aftershock law. Our point is to demonstrate that the simultaneous incorporation of aging of contacts in the sliding interface and of elasticity of the sliding plates constitutes the minimal ingredients to account for both laws within the same frictional model.

I. INTRODUCTION

Two very well known, empirically established laws of planetary scale friction (i.e., seismology) are the Gutenberg-Richter (GR) law [1] and the Omori law [2]. The former states that the number of earthquakes with magnitude $\geqslant \mathcal{M}$ scales with $\mathcal{M}$ as

$$\mathcal{N}(\mathcal{M}) \propto 10^{-b\mathcal{M}} \propto \mathcal{A}^{-2b/3}, \qquad (1)$$

where the dimensionless magnitude is defined as

$$\mathcal{M} = \tfrac{2}{3} \log_{10}(\mathcal{A}/\mathcal{A}_0), \qquad (2)$$

where $\mathcal{A}$ is a measure of the earthquake amplitude (energy released, stress drop, etc.), $\mathcal{A}_0$ is a constant, and $b \approx 1$ (or more generally $b = 0.5$–1.5 [3,4]). The Omori law describes the rate of aftershocks (in excess of the background value) at time t after the main event,

$$n(t) = K_{\mathrm{O}}/(\tau_c + t)^p, \qquad (3)$$

where K_{O} depends exponentially on the magnitude $\mathcal{M}$ of the main shock, $\log_{10} K_{\mathrm{O}} \propto \mathcal{M}$ [5], τ_c has a typical average value of about 7 h, and $p \approx 1$ (or more generally $p = 0.7$–1.5 [6]). A similar behavior (with $\Delta t \rightarrow -\Delta t$) was also reported for foreshocks [7,8]. Both the GR law and the Omori law were established through a statistical analysis of observed earthquakes. Although widely addressed and discussed theoretically [9–27], a generally accepted frictional model whose solution simultaneously accounts for both laws seems to be still lacking.

We build on the time-honored spring-block earthquake model dating back to Burridge and Knopoff (BK) [9] and subsequent work [10–14,21–24], where two rough sliding plates are coupled by a set of contacts which deform when the plates move relative to one another. The contacts are frictional, behaving as elastic springs as long as their stresses are below some threshold, breaking to reattach in a less-stressed state when the threshold is exceeded. The earthquake amplitude $\mathcal{A}$ is typically associated with the number of broken contacts at a global slip sliding event—the shock. The BK-type models do predict a GR-like power-law behavior, but typically for some particular sets of model parameters (see a detailed analysis of

BK-type models in Refs. [25,26]), and generally only for a restricted interval of magnitudes $\Delta \mathcal{M} \lesssim 2$ [21–24], unlike the much broader one observed in real earthquakes, and $\Delta \mathcal{M} > 6$ [28]. Beyond that partial failure, the existing earthquake models do not describe spatial-temporal correlations between different earthquakes and thus fail altogether to explain the Omori law. Aftershocks have been generally related to relaxation [21,22], but that aspect is still in need of proper integration with others in a single model [18,20].

We undertake that integration in the present work, where we show that a simultaneous description of both the GR law and the Omori law can be obtained by models that incorporate two main ingredients: the elasticity of the sliding plates and the aging of contacts between the plates.

II. THE MODEL

A. The sliding interface as a set of macrocontacts

As typical in earthquakelike models, we assume two plates, the top plate (the slider) and the bottom plate (the base), coupled by a multiplicity of frictional microcontacts. If an individual microcontact (asperity, bridge, solid island, etc.) has a size r_c, then its elastic constant may be estimated as $k_c \sim \rho c_t^2 r_c$, where ρ is the mass density and c_t is the transverse sound velocity of the material which forms the asperity.

Elastic theory introduces a characteristic distance λ_c known as the elastic correlation length, below which the frictional interface may be considered as rigid [29–31]. Roughly it may be estimated as $\lambda_c \sim a_c^2 E / k_c$, where a_c is an average distance between the microcontacts and E is the slider Young modulus. A set of $N_c = \lambda_c^2 / a_c^2$ microcontacts within the area λ_c^2 constitutes an effective macrocontact [31,32] with the elastic constant $k = N_c k_c \lesssim E \lambda_c$. The macrocontact is characterized by the shear force $F_i(u_i)$, where u_i is the displacement of the point on the slider to which the ith macrocontact is attached. The function $F_i(u_i)$ may be calculated with the master equation approach [33,34] provided the statistical properties of microcontacts are known. Because of a strong (Coulomblike) elastic interaction between the microcontacts at distances $r < \lambda_c$, the effective distribution of threshold values

for frictional microcontacts reduces to a narrow Gaussian distribution; i.e., it is close to the δ function [31]. In this case F_i linearly increases with u_i until the macrocontact undergoes the elastic instability [31,34–36], when (almost all) microcontacts break and the macrocontact slides.

Thus, we assume that each macrocontact (simply called contact from now on) is characterized by the shear force $F_i = ku_i$ and by the threshold value F_{si}. The contact stretches elastically so long as $|F_i| < F_{si}$, but breaks and slides when the threshold is exceeded. When a contact breaks, its shear force drops to $F_i \sim 0$, and evolution continues from there, with a new freshly assigned value for its successive breaking threshold.

The macrocontacts are elastically coupled through the deformation of the slider's bulk. The elastic energy stored between two nearest neighboring (NN) contacts, i and j, in a nonuniformly deformed slider may formally be written as $\frac{1}{2}K(u_i - u_j)^2$, where K is the slider rigidity defined below in Sec. II B. Within this multiscale theory of the frictional interface, the sliding proceeds through creation and propagation of self-healing cracks treated as solitary waves [31,32].

B. Elastic model of the sliding plate

An earthquake corresponds to a release of elastic energy accumulated in a body of the plate during its previous slow motion. Therefore, any earthquake model has to include the plate elasticity. In a majority of earthquakelike models this is done indirectly through introducing an interaction between neighboring contacts. For example, the most widely studied Olami, Feder, and Christensen (OFC) model [12] assumes that when the stress on one of the contacts reaches the threshold value σ_s, it breaks, and the accumulated stress is equally redistributed over the NN contacts, increasing their stresses on $\alpha\sigma_s$, where $\alpha < 1/4$ is a parameter. This may stimulate the NN contacts to break too, creating an avalanche of contact breaking—a large shock. The distribution of shock magnitudes in this case may follow the power law. However, such explanation of the GR law is not "robust"—the power law is observed for some sets of model parameters and for a restricted interval of earthquake magnitudes, typically much smaller than that observed in real earthquakes. Instead, the GR law may be associated with macrocontact aging alone as discussed previously [24] (see also Sec. II C).

Nevertheless, the incorporation of the plate elasticity into a realistic earthquake model is still important because, as we show in this work, it is responsible for aftershocks. When one of the macrocontacts breaks and slides, the stress on neighboring contacts increases causing them to break as well, and this process continues for some distance Λ, where the contact stress drops lower than (but close to) its threshold value. During propagation of this "breaking wave"—corresponding to a large earthquake, or the main shock—the previously accumulated elastic energy is released. But an important issue is that the stress is not completely relaxed—the region where the wave was arrested retains a stress close to the threshold value and thus represents a source for the next earthquake—the aftershock.
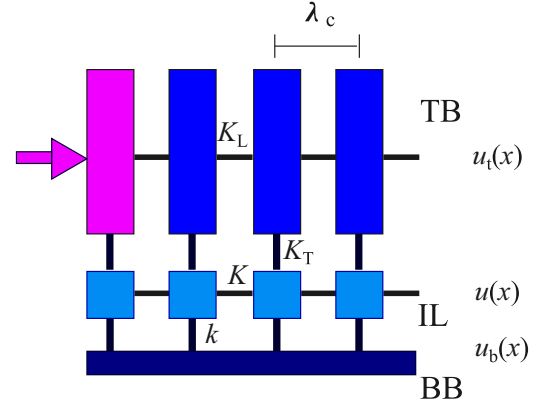

FIG. 1. (Color online) The model. The top block (TB) is split in rigid blocks of size $\lambda_c \times W \times H$ connected by springs of the elastic constant K_L. The interface layer (IL) is split in rigid blocks of size $\lambda_c \times W \times \lambda_c$ connected by springs of the elastic constant K. The TB and the IL are coupled by springs of the elastic constant K_T. The IL is connected with the rigid bottom block (BB) by contacts, represented by "frictional" springs of the elastic constant k, which break when the local stress exceeds a threshold value.

The driving force which supports the propagation of the breaking wave is the stress accumulated in the body of the plate; i.e., the latter plays the role of a "stress reservoir." Because of the long-range character of stress distribution in an elastic body (the stress decays with distance according to a power law), this effect cannot be described by OFC-like models, where the stress is localized; therefore one has to use a three-dimensional (3D) model of the plate. A full-fledge simulation of a 3D earthquake model seems still out of reach of modern computer power. Instead, here we propose the two-layer model of the sliding plate, where one layer (IL) plays the same role as in BK-type models, while the second layer (TB) plays the role of a massive tectonic plate, where the elastic stress is accumulated.

To be specific we elaborate here the simplest one-dimensional (1D) version of the model, where the contacts constitute a regular chain of length $L = Na$ with the spacing $a = \lambda_c$ as shown schematically in Fig. 1 [see Appendix A for how the 1D model may be "deduced" from the 3D elastic model of the plate and the corresponding parameters, Eqs. (4)–(6) below, defined]. The base (the bottom block BB) is assumed to be rigid, whereas the elastic top plate (the top block TB, the slider) of length L, width W (in our 1D model we must set $W = \lambda_c$), and an effective height (thickness) H is modeled by the chain of $N = L/a$ rigid blocks coupled by springs of elastic constant

$$K_L = E\lambda_c (H/\lambda_c) \tag{4}$$

(note that $H \gg \lambda_c$ must hold for the correlation length λ_c to be defined). The contact between the TB and the BB is described as an interface layer (IL) of thickness $H_c \sim \lambda_c$, consisting of N contacts coupled by springs with elastic constant

$$K = E\lambda_c. \tag{5}$$

The IL and the TB are coupled elastically with a transverse rigidity which we model by N springs of elastic constant

$$K_{\text{T}} = \frac{E\lambda_c}{2(1+\sigma_{\text{P}})} \frac{\lambda_c}{H}, \tag{6}$$

where σ_{P} is the slider Poisson ratio. Finally, the IL is coupled "frictionally" with the top surface of the BB—each contact between the two plates is elastic with stiffness constant k as long as the local shear stress in the IL is below the threshold. The interface is stiff if $k \gtrsim K$ and soft when $k \ll K$; here we concentrate on the latter case.

Now, if a lateral pushing force is applied, for example, to the left-hand side of the slider as shown in Fig. 1, the stress is transmitted to each contact due to the elasticity of the slider. In this case the interface dynamics starts by relaxation of the leftmost contact which initiates the sliding. This causes an extra stress on the neighboring contacts, which tend to slide too, and the domino of sliding events propagates as a solitary wave [31,32], extending the relaxed domain, until the stress at some contact falls below the threshold. Such a self-healing crack propagates for some characteristic length Λ—leaving a relaxed stress behind its passage, but raising the interface shear stress ahead of the crack. The value of Λ may be estimated analytically [37]; roughly Λ/a is proportional to H/λ_c as well as to k/K.

C. Aging of the sliding interface

The importance of incorporation of interface aging—an effective strengthening of the interface due to slow relaxations, growth of the contact sizes, or their gradual reconstruction, chemical "cementation," etc.—is well known for earthquake modeling as well as for tribological studies [26]. In particular, aging is held responsible for a well-known effect—the transition from stick-slip to smooth sliding with changing of the sliding velocity v [38]. Typically aging is accounted for phenomenologically by assuming that the friction force decreases when v increases (the velocity-weakening hypothesis). At the simplest level, one may just postulate the existence of two coefficients, the static friction coefficient μ_s for the pinned state and the kinetic friction coefficient $\mu_k < \mu_s$ for the sliding state.

In the earthquakelike model, where the contacts continuously break and reform, it is natural to assume that newborn contacts have initially a small (e.g., zero) breaking threshold which then grows with the lifetime of the pinned contact. In the simplest variant one may introduce simply a delay time by assuming that the contact reappears after some time τ_d (so that for times $t < \tau_d$ the threshold is zero).

In our model, where one macrocontact is represented by many microcontacts which break and reform, it is natural to assume that the macrocontact possesses its own internal dynamics corresponding to a stochastic process. Let F_{si} be a threshold value for contact i. Even assuming, as we do, that newborn contacts emerge with a vanishing breaking threshold $F_{si} \sim 0$, that threshold value will grow with time due to contact aging. We assume that the stochastic evolution of contact thresholds is described by the simplest Langevin equation:

$$dF_{si}(t)/dt = K(F_{si}) + G\,\xi(t), \tag{7}$$

where $K(F_{si})$ and G are the so-called drift and stochastic forces, respectively [39], and $\xi(t)$ is the Gaussian random force, $\langle\xi(t)\rangle = 0$ and $\langle\xi(t)\xi(t')\rangle = \delta(t - t')$. Equation (7) is equivalent to the Fokker-Planck equation for the distribution of thresholds $\mathcal{P}_c(F_{si}; t)$ (see Appendix B):

$$\frac{\partial\mathcal{P}_c}{\partial t} + \frac{dK}{dF_{si}}\mathcal{P}_c + K\frac{\partial\mathcal{P}_c}{\partial F_{si}} = \frac{1}{2}G^2\frac{\partial^2\mathcal{P}_c}{\partial F_{si}^2}. \tag{8}$$

Our main assumption, Ref. [24], is that the drift force is given by

$$K(F_{si}) = \left(\frac{2\pi F_s}{\tau_0}\right)\beta^2\frac{1 - F_{si}/F_s}{1 + \varepsilon(F_{si}/F_s)^2}, \tag{9}$$

while the amplitude of the stochastic force is

$$G = (4\pi/\tau_0)^{1/2}\beta\delta F_s, \tag{10}$$

where β and ε are two dimensionless parameters, and the model parameters τ_0, F_s, and $\delta \equiv \delta F_s/F_s$ define the space-time scale and are fixed below in Sec. III.

With this choice, the stationary solution $\mathcal{P}_{c0}(F_{si})$ of Eq. (8) corresponds to the Gaussian distribution $\mathcal{P}_{c0}(F_{si}) = (2\pi)^{-1/2}(\delta F_s)^{-1}\exp[-\frac{1}{2}(1 - F_{si}/F_s)^2/\delta^2]$ in the case of $\varepsilon = 0$, while for $\varepsilon > 0$ the threshold distribution has a power-law tail, $\mathcal{P}_{c0}(F_{si}) \propto F_{si}^{-1/\varepsilon\delta^2}$ for $F_{si} \gg F_s$. Therefore, the dimensionless parameter ε determines the deviation of the threshold distribution from the Gaussian shape, while β corresponds to the rate of aging.

The stochastic dynamics alone leads to the power-law distribution of thresholds in the stationary state. Thus, if the plate moves adiabatically, $v \to 0$, then at $t \to \infty$ the distribution of earthquake magnitudes will follow the GR-like law even for $\mathcal{M} \to \infty$. However, when $v > 0$, there is a competition between the growing process and the continuous contact breaking due to sliding, and the maximal magnitude of earthquakes is restricted. For the steady state motion the corresponding solution may be found analytically with the master equation approach [24]; it gives

$$\mathcal{M}_{\max} \propto \log_{10}(\beta/\sqrt{v}). \tag{11}$$

III. SIMULATION

In simulations we typically used a chain of $N = 901$ macrocontacts with the periodic boundary condition. Four parameters of our model may be fixed without loss of generality: $a = 1$ (the length unit), $K = 1$, $m = 1$ (mass of the macrocontact), and $F_s = 1$. Then, the characteristic frequency is $\omega_0 = (K/m)^{1/2} = 1$, so that the unit of time is $\tau_0 = 2\pi/\omega_0 = 2\pi$.

For the elastic slider we used $N_{\text{L}} \equiv H/\lambda_c = 100$ so that $K_{\text{L}} = N_{\text{L}}K$ and $K_{\text{T}} = K/(2.6\,N_{\text{L}})$. We took $\sigma_{\text{P}} = 0.3$ for the Poisson ratio, and $M = N_{\text{L}}m$ for the mass of TB blocks. The top layer of the slider is driven through springs attached to the TB blocks, each with the elastic constant $K_d = 0.03K$, the springs ends moving with the constant velocity $v = 0.01$. In simulations, the contacts' elastic constant is $k = 0.03K$ and the thresholds' dispersion parameter $\delta F_s = 0.1F_s$; that yields a characteristic distance for self-healing crack propagation $\Lambda \lesssim 100a$ [37]. A contact aging parameter $\varepsilon = 75$ yields a GR distribution with $b \approx 1$ (see Ref. [24]); a reasonable rate of

aging is chosen as $\beta = 1$. The newborn contacts emerge with the threshold F_{si} taken from the Gaussian distribution with the average $F_{s,\text{nb}} = 0.01 F_s$ and the deviation $\delta F_{s,\text{nb}} = F_{s,\text{nb}}$. In the initial state, all contacts are relaxed, $F_i = 0$, and all thresholds correspond to newborn contacts. Then, the equations of motion for all blocks (with a viscous damping coefficient $\eta = 1$) together with the Langevin equations for contact breaking thresholds are solved with the time step $\Delta t = 0.01$. The total simulation time required is $t_{\text{max}} = 2 \times 10^7$ (taking a typical velocity of a tectonic plate $v \sim 30$ mm/yr $\approx 3 \times 10^{-9}$ m/s and a distance between the contacts $a \sim 1$ mm, we obtain that the time step $\Delta t = 0.01$ in simulation with $a = 1$ and $v = 0.01$ corresponds to a real-time step ~ 30 s and the total time $\sim 6 \times 10^{10}$ s $\sim 2 \times 10^3$ yr). In contrast to the cellular automaton algorithm typically used in simulations of the BK model [9], in the present work we use, following Carlson and Langer [10], an alternative algorithm with a fixed time step Δt. Although in this case more than one contact breaking event may take place in a single time step (which corresponds to an earthquake in our model with "living" macrocontacts) that does not alter our main results (e.g., see discussion in Ref. [24]). We define the (dimensionless) quake amplitude as the sum of force drops on contacts at every time step,

$$\mathcal{A}(t) = \sum_i \Delta F_i(t)/F_s, \qquad (12)$$

and the rate of shocks $n(t)$ as the number of shocks per one time step (regardless of their amplitude).

The results are presented in Figs. 2 and 3. A typical time sequence of earthquake shock sizes is that of Fig. 2(b). On a large time scale, the function $\mathcal{A}(t)$ appears stochastic. On a finer scale though [Fig. 3(b)] one can distinguish separated
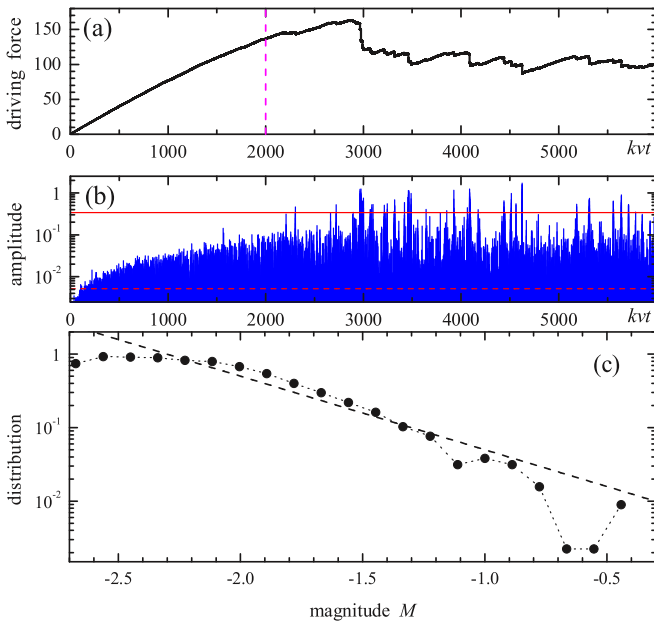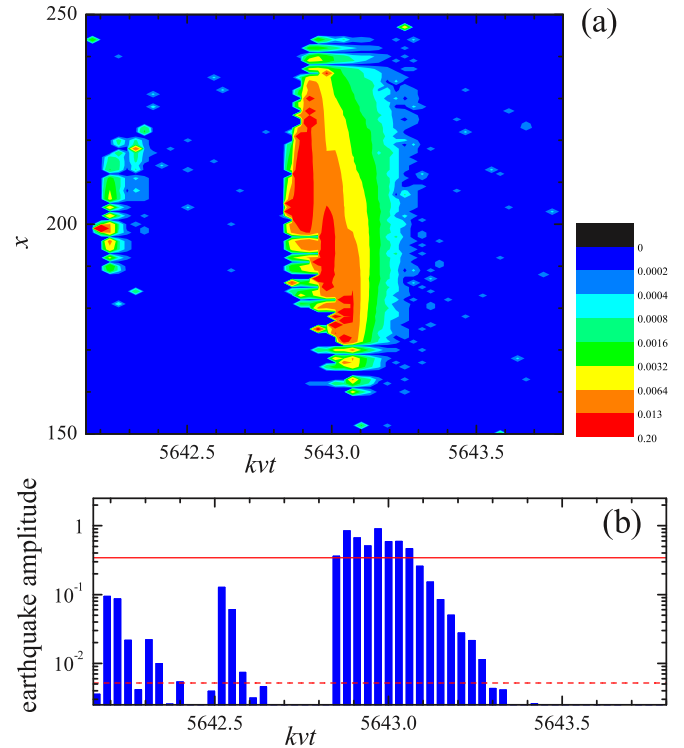

FIG. 3. (Color online) Typical earthquake in our model: (a) the color map of the earthquake amplitude on the (t,x) plane, and (b) the earthquake amplitude $\mathcal{A}(t)$ versus time.

shock blocks, each with a large main shock followed by aftershocks.

IV. ANALYSIS OF RESULTS

We can now analyze the earthquake shocks for their characteristics, distribution, and correlations in space and time. To do that efficiently, we first remove from the analysis the small "background" earthquakes with amplitudes below some level—we retain only $\mathcal{A} > 2 \langle \mathcal{A}(t) \rangle$ [broken red line in Figs. 2(b) and 3(b)]. Next, we single out the main earthquakes above some level $\mathcal{A}_{\text{MEQ}}$; we took here $\mathcal{A}_{\text{MEQ}} = 0.2 \mathcal{A}_{\text{max}}$ [red solid line in Figs. 2(b) and 3(b)]. We also used the following rescaling procedure to distinguish from one another main earthquakes that may occur too close: If n_{MEQ} is the total number of main earthquakes, call $\sigma = S/n_{\text{MEQ}}$ the average area occupied by a single main earthquake on the (t,x) plane, with $S = t_{\text{max}} L$. We then rescale the time coordinate $t \rightarrow \tau = t/\alpha$ with $\alpha = \sigma/\lambda^2$, where λ is some distance chosen in such a way that the distribution of main earthquakes on the (τ,x) plane becomes *isotropic* ($\lambda \approx 235$ for the parameters used in Fig. 2). We can now scan all main earthquake coordinates on the (τ,x) plane and, if the distance $\rho_{ij} = [(\tau_i - \tau_j)^2 + (x_i - x_j)^2]^{1/2}$ between two main earthquakes i and j is smaller than some value ρ_{cut} (we chose $\rho_{\text{cut}} = 0.75 \lambda$), then only the larger of these two main earthquakes remains as the main earthquake, while the lower one is removed from the list of main earthquakes.

With this protocol we have obtained a set of well-separated main earthquakes isotropically occupying the (τ,x) plane, and

FIG. 2. (Color online) Time evolution of the system: (a) the frictional force $F(t)$, and (b) the (global) amplitude of earthquakes $\mathcal{A}(t)$ versus time. (c) Statistics of earthquake magnitudes presented in panel (b) (the first 33% of data discarded) showing the GR power-law behavior; the dashed line corresponds to the exponent $b = 1$.

we may calculate the temporal and spatial distribution of all earthquakes within some area around every main earthquake—we count the earthquakes separated from the corresponding main earthquake by less than $\rho_0 = \rho_{cut}/3$. Then we collapse all data together, designating $\tau = 0$ for every main shock and normalizing shock amplitudes on the corresponding main shock value (because the data so obtained are still noisy, we coarsened the distribution with an extra width $\Delta\rho$ in the (τ, x) plane, using $\Delta\rho = \rho_0/31$).

The earthquake distribution—our main result—is presented in Fig. 4. One can clearly see that the aftershocks satisfy the Omori law (Fig. 4). The number of aftershocks [the coefficient K_O in the Omori law (3)] depends exponentially on the magnitude $\mathcal{M}$ of the corresponding main shock [Fig. 4(c)], although the numerical coefficient of the exponent ($\sim 9/2$) is essentially larger than that reported for real earthquakes ($\sim 1/2 - 2/3$, see Ref. [5]); this may be connected with the fact that the "earthquake amplitude" $\mathcal{A}$ defined in our 1D model is not exactly equivalent to the seismic moment M_O used in the analyzing of earthquake statistics. The spatial correlation between the shocks decays exponentially in our 1D model unlike in real earthquakes, where the aftershock amplitude decays the power law with distance owing to 3D elasticity [40]; since the origin of that discrepancy is so very clear, it

does not worry us. Foreshocks are also observed in simulation, typically with a smaller value of the lag time τ_c.

V. CONCLUSIONS

The spring-block frictional model elaborated and solved in this article confirms and details the mechanism through which elasticity of the sliding plates and contact aging enter as the key ingredients of a minimal earthquake model. Without either of them, the coexistence of the GR power-law energy distribution with Omori's power-law aftershock distribution would not occur. In the earlier model of Ref. [24] it was shown instead how the GR earthquake law could arise due to contact aging alone. Explicit incorporation of the slider's elasticity done here provides also the spatial-temporal distribution of earthquakes in fair accordance with the Omori aftershock law.

The magnitude of the largest earthquake is controlled in the present model by the parameter β, the rate of aging relative to the driving velocity. The spatial radius of aftershock activity is controlled by the length Λ, the self-healing crack propagation distance.

As a sobering remark in closing, stimulated by one reviewer, we should observe that the present modeling has no pretense to represent the full complexity of real earthquakes. In experimental aftershock sequences the first aftershock has usually a magnitude one unity smaller than the main shock (Bath's law [41]) whereas in the numerical result [Fig. 3(b)] we have clusters of consecutive earthquakes with about the same amplitudes. Also, the dependence of the coefficient K_O in the Omori law on the main shock magnitude is poorly reproduced in the present 1D model. Besides, the true number of foreshocks is typically much smaller than that obtained here (Fig. 4).

Future improvements of the model will clearly be needed to account for these additional aspects, besides the very basic ones which it presently deals with. The study of a 2D model of the interface and a 3D model of the elastic slider would provide a power-law earthquake spatial distribution. More generally we think one can build on this basic modeling and describe, through extensions and adjustment of model parameters and ingredients, the greater complexity of real earthquakes.

APPENDIX A: TWO-LAYER MODEL OF THE ELASTIC PLATE

There is no way to reduce the 3D elastic model of the tectonic plate to a 1D model rigorously, but one may define a 1D model that leads to qualitatively reasonable results. Let us consider the 3D elastic slider of size $L \times W \times \widetilde{H}$ with the longitudinal rigidity $\mathcal{K} = E W \widetilde{H}/L$ and the transverse rigidity $\mathcal{K}_T = [E/2(1 + \sigma_P)](LW/\widetilde{H})$. For numerical study, we split
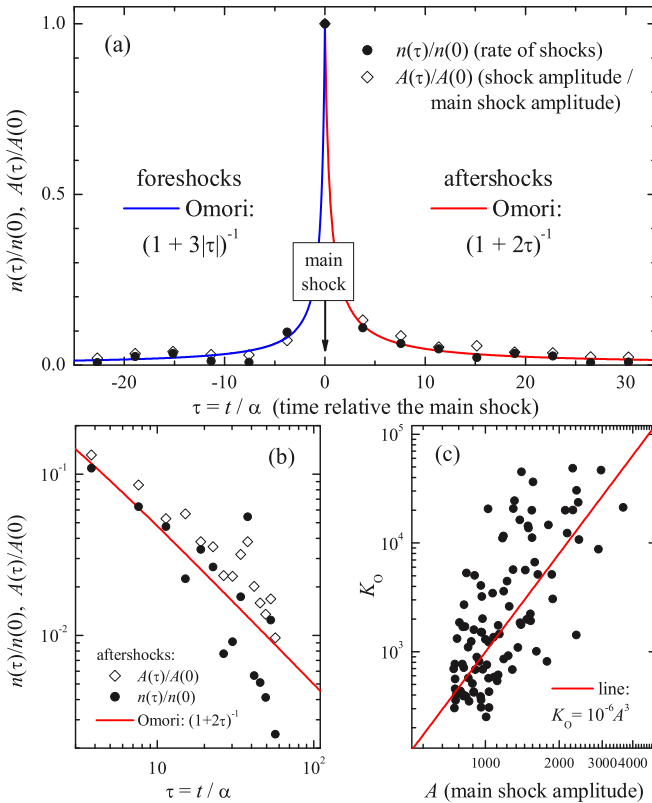

FIG. 4. (Color online) (a) Foreshock and aftershock statistics: the rate of fore- and aftershocks $n(\tau)$ (solid circles) and the shock amplitudes $\mathcal{A}(\tau)$ (open diamonds) relative to the corresponding main shock. The curves demonstrate the Omori law. (b) Aftershock statistics in log-log scale. (c) The coefficient K_O in Eq. (3) as a function of the amplitude of the main shock in log-log scale. The line shows the $K_O \propto \mathcal{A}^3 \propto 10^{4.5\mathcal{M}}$ dependence.
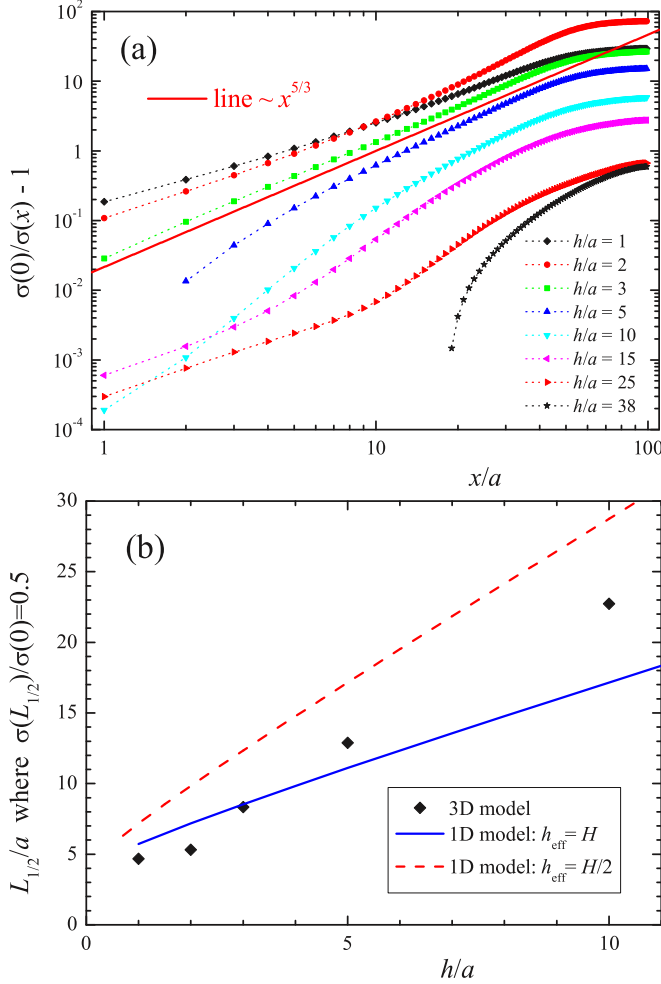
FIG. 5. (Color online) (a) The shear stress σ in the interface versus x for the 3D slider of size $100a \times 3a \times 38a$ with the mass density $\rho = 1.19 \times 10^3$ kg/m^3, the sound speeds $c_l = 2680$ m/s and $c_t = 1100$ m/s (the parameters corresponding to Plexiglass experimentally studied in Ref. [43]), and $k/K = 0.03$. (b) Dependence of the length $L_{1/2}$ on the height of the applied pushing force h (symbols, numerics); lines show the 1D model dependencies $L_{1/2}(h_{\text{eff}})$ with $h_{\text{eff}} = H$ (blue solid line) and $h_{\text{eff}} = H/2$ (red dashed line).

it into cubes of linear size a. The interaction between the NN cubes in the isotropic case is described by two constants, the longitudinal elastic constant $\kappa_l = \rho c_l^2 a$ and the transverse one, $\kappa_t = \rho c_t^2 a$, where ρ is the mass density and c_l (c_t) is the longitudinal (transverse) sound speed [42].

Then, let the slider be coupled with the rigid bottom plate by LW/a^2 springs of elastic constant k. If we now apply the pushing force from the left-hand side of the slider at a height of $h < \widetilde{H}$, it will produce the stress $\sigma(x)$ at the slider-BB interface (we consider the system uniform in the y direction, along which we apply the periodic boundary condition). The function $\sigma(x)$ for the 3D slider roughly follows a power law, $\sigma(x) \propto x^{-\nu}$, where the exponent $\nu < 3$ depends on model parameters [see Fig. 5(a)]. To characterize the decaying function $\sigma(x)$, we define the length $L_{1/2}$ where the stress decreases in two times, $\sigma(L_{1/2})/\sigma(0) = 0.5$. Figure 5(b) shows the dependence of $L_{1/2}$ on the height h where the

pushing force is applied. Of course, a 1D model cannot reproduce the power-law dependence; the 1D model always gives the exponentially decaying stress distribution. Our idea is to construct an effective 1D model that leads to a qualitatively similar dependence of $L_{1/2}$ on model parameters.

Let us consider the lowest layer of the slider as the IL so that it corresponds to a chain of $N = L/a$ cubes coupled with the BB by springs k and connected between themselves by springs $K = \kappa_l = Ea$, Eq. (5) (in a general case one may put $K = \kappa_l E_c/E$, where E_c is the Young modulus of the interface, but we do not see reasons to introduce additional parameters in our qualitative 1D model).

Then, let us connect rigidly in the z direction the remaining $N_z = H/a$ ($H = \widetilde{H} - a$) layers of the slider, so that it now consists of N rigid blocks coupled by springs of elastic constant $K_L = N\mathcal{K} = EH$, Eq. (4), as shown in Fig. 1. Finally, to reproduce the slider transverse rigidity $\mathcal{K}_T$, we couple the IL and the TB by N springs of elastic constant $K_T = \mathcal{K}_T/N$, which gives Eq. (6) (one may think that we have to put $K_T = \kappa_t$, but this choice does not simulate correctly the slider transverse rigidity and does not reproduce the dependence of $L_{1/2}$ on model parameters qualitatively similar to that of 3D numerics).

Thus, we came to the effective 1D model of the slider described in Sec. II B, Fig. 1. This model allows us to find analytically the stress distribution along the interface, $\sigma(x) \propto \exp(-\kappa_2 x)$, where

$$\kappa_2^2 = \tfrac{1}{2}\left[(\kappa^2 + \kappa_T^2) - \sqrt{\mathcal{D}}\,\right], \tag{A1}$$

$$\mathcal{D} = (\kappa^2 - \kappa_T^2)^2 + 4\beta\kappa^2\kappa_T^2, \tag{A2}$$

$$(a\kappa_T)^2 = K_T/K_L, \tag{A3}$$

$$(a\kappa)^2 = (k + K_T)/K, \tag{A4}$$

$$\beta = K_T/(K_T + k), \tag{A5}$$

so that now $L_{1/2} = (\ln 2)/\kappa_2$. The comparison of the 1D analytical dependence $L_{1/2}(H)$ with the 3D numerical one $L_{1/2}(h)$ is presented in Fig. 5(b). One can see that, if we interpret the parameter H in our 1D model as some effective thickness of the tectonic plate where the elastic stress is accumulated, we could obtain qualitative correct results. Moreover, the 1D model allows us to find analytically the characteristic length Λ—the propagation path of the self-healing crack—which determines the distance where the stress remains unrelaxed (and even increases to become close to the threshold) after a large shock and, therefore, where an aftershock could occur.

Thus, our 1D model of the slider is characterized by two dimensionless parameters: k/K defines the stiffness of the interface, and H/a determines the "capacity" of the tectonic plate, where the elastic stress is accumulated.

APPENDIX B: AGING OF THE CONTACTS

The Langevin equations (7) for the thresholds F_{si} have to be solved numerically. For example, if at $t = 0$ the threshold is zero, then the average threshold value will grow with time according to the power law $\langle F_{si} \rangle \propto t^\nu$ at short times as demonstrated in Fig. 6, where the value of the exponent $\nu \leqslant 0.5$ depends on the parameter ε. For $\varepsilon\delta^2 < 0.5$ the average threshold
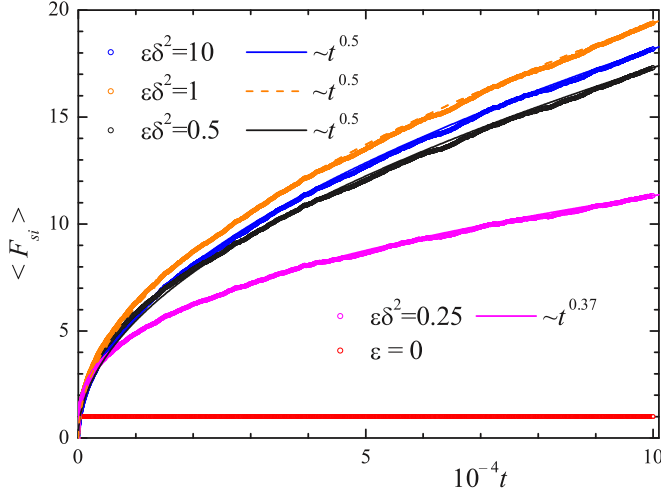
FIG. 6. (Color online) Macrocontact aging: growth of the contact threshold $\langle F_{si} \rangle$ with its timelife for $\beta = 0.3$, $\delta = 0.1$, and $\varepsilon = 0, 25, 50, 100$, and 1000 (see legend). Curves show power-law fits.

$\langle F_{si} \rangle = \int_0^\infty dF\, F \mathcal{P}_c(F;t)$ tends to saturate to a finite value at $t \to \infty$, while for $\varepsilon\delta^2 \geqslant 0.5$ it keeps growing with time.

Now let us derive the corresponding Fokker-Planck equation which will allow us to find some analytical results. Equation (7) is equivalent to the stochastic equation [39]

$$dF_{si}(t) = K(F_{si})dt + Gdw, \qquad (B1)$$

where

$$\langle dw \rangle = 0,$$
$$\langle dw(t)\, dw(t) \rangle = dt. \qquad (B2)$$

Let us introduce the distribution function $\mathcal{P}_c(F_{si}, t|F_{si0}, t_0)$ defined as the conditional probability that the contact i has the threshold F_{si} at time t, if at the previous time t_0 it had the value F_{si0}. For an arbitrary function $u(F_{si})$, its average value $\langle u \rangle$ at time t is equal to

$$\langle u \rangle = \int dq\, u(q) \mathcal{P}_c(q, t|\cdots), \qquad (B3)$$

and its derivative over time is

$$\frac{d}{dt}\langle u \rangle = \int dq\, u(q) \frac{\partial \mathcal{P}_c(q, t|\cdots)}{\partial t}. \qquad (B4)$$

On the other hand, the differential of the function $u(q)$ with an accuracy up to dt, with the help of Eq. (B1), may be written in the form

$$\begin{aligned}
du &= (\partial u/\partial F_{si})dF_{si} + \tfrac{1}{2}(\partial^2 u/\partial F_{si}^2)dF_{si}dF_{si} \\
&= (\partial u/\partial F_{si})[K(F_{si})dt + Gdw(t)] \\
&\quad + \tfrac{1}{2}(\partial^2 u/\partial F_{si}^2)G^2 dw(t)dw(t), \qquad (B5)
\end{aligned}$$

where the second derivative appears because $\langle dw \rangle \sim \sqrt{dt}$ in the stochastic equation.

Averaging Eq. (B5) over time using the Ito calculus [39], dividing both sides of the equation by dt, and taking into account Eqs. (B2), we obtain

$$\frac{\langle du \rangle}{dt} = \left\langle \frac{\partial u}{\partial F_{si}} K(F_{si}) \right\rangle + \frac{1}{2}\left\langle \frac{\partial^2 u}{\partial F_{si}^2} G^2 \right\rangle. \qquad (B6)$$

The first term in the right-hand side of Eq. (B6) may be rewritten as

$$\begin{aligned}
\left\langle \frac{\partial u}{\partial F_{si}} K(F_{si}) \right\rangle &= \int dq\, \mathcal{P}_c(q, t|\cdots) K(q) \frac{\partial u}{\partial q} \\
&= -\int dq\, u(q) \frac{\partial}{\partial q}[K(q)\mathcal{P}_c(q, t|\cdots)], \quad (B7)
\end{aligned}$$

where we also made the integration by parts. In a similar way the second term in the right-hand side of Eq. (B6) may be transformed, if we make the integration by parts two times. Then, comparing the obtained expression for $\langle du \rangle/dt$ with Eq. (B4) and taking into account that the function $u(q)$ is an arbitrary one, we obtain that the distribution function $\mathcal{P}_c(F_{si}, t|\cdots)$ must satisfy the following equation:

$$\begin{aligned}
\frac{\partial \mathcal{P}_c(F_{si}, t|\cdots)}{\partial t} &= -\frac{\partial}{\partial F_{si}}[K(F_{si})\mathcal{P}_c(F_{si}, t|\cdots)] \\
&\quad + \frac{1}{2}\frac{\partial^2}{\partial F_{si}^2}[G^2 \mathcal{P}_c(F_{si}, t|\ldots)], \qquad (B8)
\end{aligned}$$

which is the Fokker-Planck equation (8).

[1] B. Gutenberg and C. F. Richter, *Seismicity of the Earth and Associated Phenomena* (Princeton University Press, Princeton, NJ, 1954); Bull. Seismol. Soc. Am. **46**, 105 (1954).

[2] F. Omori, J. Coll. Sci., Imp. Univ. Tokyo **7**, 111 (1894).

[3] J. B. Rundle *et al.*, Rev. Geophys. **41**, 1019 (2003).

[4] L. Gulia and S. Wiener, Geophys. Res. Lett. **37**, L10305 (2010).

[5] Y. Yamanaka and K. Shimazaki, J. Phys. Earth **38**, 305 (1990).

[6] T. Utsu, Y. Ogata, and R. S. Matsu'ura, J. Phys. Earth **43**, 1 (1995).

[7] Y. Y. Kagan and L. Knopoff, Geophys. J. R. Astron. Soc. **55**, 67 (1978).

[8] L. M. Jones and P. Molnar, J. Geophys. Res. **84**, 3596 (1979).

[9] R. Burridge and L. Knopoff, Bull. Seismol. Soc. Am. **57**, 341 (1967).

[10] J. M. Carlson and J. S. Langer, Phys. Rev. Lett. **62**, 2632 (1989); Phys. Rev. A **40**, 6470 (1989).

[11] H. Nakanishi, Phys. Rev. A **41**, 7086 (1990).

[12] Z. Olami, H. J. S. Feder, and K. Christensen, Phys. Rev. Lett. **68**, 1244 (1992).

[13] J. E. S. Socolar, G. Grinstein, and C. Jayaprakash, Phys. Rev. E **47**, 2366 (1993).

[14] P. Grassberger, Phys. Rev. E **49**, 2436 (1994).

[15] J. B. Rundle and W. Klein, Nonlinear Processes Geophys. **2**, 61 (1995).

[16] J. R. Rice and Y. Ben-Zion, Proc. Natl. Acad. Sci. USA **93**, 3811 (1996).

[17] R. S. Stein, Nature (London) **402**, 605 (1999).

[18] S. Hergarten and H. J. Neugebauer, Phys. Rev. Lett. **88**, 238501 (2002).

[19] M. S. Mega, P. Allegrini, P. Grigolini, V. Latora, L. Palatella, A. Rapisarda, and S. Vinciguerra, Phys. Rev. Lett. **90**, 188501 (2003).

[20] S. Hergarten and R. Krenn, Nonlinear Processes Geophys. **18**, 635 (2011).

[21] S. Hainzl, G. Zöller, and J. Kurths, J. Geophys. Res. **104**, 7243 (1999); Nonlinear Processes Geophys. **7**, 21 (2000).

[22] E. A. Jagla, Phys. Rev. E **81**, 046117 (2010); E. A. Jagla and A. B. Kolton, J. Geophys. Res.: Solid Earth **115**, B05312 (2010).

[23] C. A. Serino, K. F. Tiampo, and W. Klein, Phys. Rev. Lett. **106**, 108501 (2011).

[24] O. M. Braun and M. Peyrard, Phys. Rev. E **87**, 032808 (2013).

[25] J. D. Pelletier, Geophys. Monogr. **120**, 27 (2000).

[26] H. Kawamura, T. Hatano, N. Kato, S. Biswas, and B. K. Chakrabarti, Rev. Mod. Phys. **84**, 839 (2012).

[27] E. A. Jagla, Phys. Rev. Lett. **111**, 238501 (2013).

[28] Y. Ben-Zion and J. R. Rice, J. Geophys. Res. **100**, 12959 (1995).

[29] C. Caroli and Ph. Nozieres, Eur. Phys. J. B **4**, 233 (1998).

[30] B. N. J. Persson and E. Tosatti, Solid State Commun. **109**, 739 (1999).

[31] O. M. Braun, M. Peyrard, D. V. Stryzheus, and E. Tosatti, Tribol. Lett. **48**, 11 (2012).

[32] O. M. Braun and M. Peyrard, Phys. Rev. E **85**, 026111 (2012).

[33] O. M. Braun and M. Peyrard, Phys. Rev. Lett. **100**, 125501 (2008).

[34] O. M. Braun and M. Peyrard, Phys. Rev. E **82**, 036117 (2010).

[35] O. M. Braun and E. Tosatti, Europhys. Lett. **88**, 48003 (2009).

[36] O. M. Braun and E. Tosatti, Philos. Mag. **91**, 3253 (2011).

[37] O. M. Braun and J. Scheibert (unpublished).

[38] B. N. J. Persson, *Sliding Friction: Physical Principles and Applications* (Springer-Verlag, Berlin, 1998).

[39] C. W. Gardiner, *Handbook of Stochastic Methods for Physics, Chemistry and the Natural Sciences* (Springer-Verlag, Berlin, 1985).

[40] K. R. Felzer and E. E. Brodsky, Nature (London) **441**, 735 (2006).

[41] M. Bath, Tectonophysics **2**, 483 (1965).

[42] L. D. Landau and E. M. Lifshitz, *Theory of Elasticity. Course of Theoretical Physics*, Vol. 7 (Pergamon, New York, 1986).

[43] S. M. Rubinstein, I. Barel, Z. Reches, O. M. Braun, M. Urbakh, and J. Fineberg, Pure Appl. Geophys. **168**, 2151 (2011).